Direct 3D extreme rainfall risk mapping from urban aerial LiDAR point clouds

Jesús Balado[1], Filip Biljecki[2]

[1]CINTECX, Universidade de Vigo, Geotech research group, Spain – jbalado@uvigo.gal
[2]Department of Architecture, National University of Singapore, Singapore –filip@nus.edu.sg

Keywords: Aerial Laser Scanning, point clouds, flood, water management, hazards, urban environment.

Abstract

Flooding is one of the most frequent and damaging natural hazards, increasingly intensified by rapid urbanization and extreme precipitation events. Accurate modelling of water accumulation and runoff in dense urban environments remains challenging due to complex geometries and the limitations of conventional surface-based representations. Most approaches require extensive LiDAR preprocessing before hydrological analysis. This study introduces a methodology for direct flood risk analysis on Aerial Laser Scanning (ALS) point clouds, avoiding intermediate surface reconstruction steps. The proposed approach enriches points with indicators of water accumulation and surface runoff potential. Water accumulation is estimated through elevation differences within a 100-m local neighbourhood to detect topographic depressions, while runoff potential is derived from three geometric descriptors (verticality, planarity, and scattering) that describe the capacity of urban structures to channel or obstruct water flow. The method was evaluated using open ALS datasets from three cities with contrasting urban morphologies: Vigo (Spain), Rotterdam (The Netherlands), and Hong Kong (China). Results demonstrate the capacity of the enriched point clouds to identify flood-prone urban features such as low-lying harbour areas, semi-tunnels, and urban canyons, as well as runoff pathways including sloped roofs, stairways, ramps, and road surfaces. The resulting point-level risk representation shows strong agreement with historical flood events and traditional multi-criteria assessments. By using LiDAR point clouds as an analytical medium, the framework enables intuitive 3D flood risk mapping while preserving their geometric richness.

1. Introduction

Flooding represents one of the most frequent and destructive natural hazards, resulting in devastating consequences for human life and global economies (Spiridonov et al., 2025). In highly urbanized regions, this concern is exacerbated by rapid population growth, aging infrastructure, and alterations in land cover. Specifically, urbanization converts permeable surfaces into impermeable ones, significantly reducing the soil's capacity for infiltration and increasing runoff, which often leads to pluvial flooding when heavy rainfall exceeds the capacity of drainage systems (Öztürk et al., 2024). Given that these impacts are projected to intensify due to climate change, the scientific and policy focus has shifted from mere flood protection to comprehensive flood risk management. Effective management requires a shared understanding of risk among stakeholders, which depends on the accurate identification of inundation zones and the precise modelling of flow dynamics within complex urban environments (Costabile et al., 2021).

To address these challenges, recent research has increasingly turned to 3D geospatial data to overcome the limitations of traditional coarse resolution 2D mapping. High-resolution LiDAR technology, particularly in the form of Airborne Laser Scanning (ALS) and UAV-borne LiDAR, has emerged as a critical tool for capturing the topographical structures that dictate floodwater pathways (Trepekli et al., 2022). For instance, UAV-LiDAR systems allow for the generation of ultra-high-resolution Digital Terrain Models (DTMs) featuring buildings at resolutions as fine as 0.3 m, which can identify obstacles like boundary walls and archways that coarser 10 m satellite models overlook. Furthermore, researchers have utilized high-resolution point clouds to simulate complex hydrological processes, such as canopy interception and soil infiltration, providing a more realistic quantification of surface flow accumulation (Baptista et al., 2018; Huang et al., 2023).

Integrating 3D datasets into hydrological models has proven essential for identifying localized risk zones. High-resolution digital surface models derived from ALS data are used to simulate flash floods in contact zones between agricultural land and residential areas (Tokarčík and Hofierka, 2024), accurately replicating real-world spillover events. Similarly, the fusion of ALS and Terrestrial Laser Scanning (TLS) has been proposed to enhance risk perception by creating 3D flood hazard maps and to visualize water levels in relation to vertical surfaces like building façades and human silhouettes (Costabile et al., 2021).

The objective of this study is to generate 3D flood risk maps directly on point clouds. Using ALS data, two types of flood-related information are derived and assigned to the points: surface runoff and water accumulation. The proposed method is tested on point clouds from three cities (Vigo, Rotterdam, and Hong Kong) representing different urban typologies and point-cloud densities.

The remainder of this paper is structured as follows. Section 2 reviews the current state of the art in flood mapping with particular emphasis on LiDAR and point cloud–based approaches. Section 3 describes the proposed methodology. Section 4 presents and discusses the results. Finally, Section 5 concludes the study.

2. Related Work

2.1 Flood Mapping and Hazard Assessment

Modern flood risk mapping is determined by the interplay of climatic, topographical, and socio-economic factors (Li et al., 2023). Primary hazard triggers include extreme precipitation intensity, low elevation, gentle slopes that facilitate water accumulation, and high drainage density (Singha et al., 2025).

This contribution has been peer-reviewed. The double-blind peer-review was conducted on the basis of the full paper.
https://doi.org/10.5194/isprs-annals-XII-4-W1-2026-33-2026 |

Exposure is largely driven by anthropogenic factors, particularly urbanization and Land Use/Land Cover (LULC) changes that increase impervious surfaces and surface runoff (Waghwala and Agnihotri, 2019). Vulnerability assessments incorporate critical socio-economic indicators such as population density, dwelling quality, household income, and road network density, which collectively determine the community's capacity to withstand and recover from flood events (Rehman et al., 2019).

The assessment and mapping of flood risks have evolved from traditional hydraulic modelling toward holistic frameworks that define combine hazards, exposures, and vulnerabilities (Bui et al., 2023; Taromideh et al., 2022). Conventional methodologies rely on physically-based hydrodynamic models, such as HEC-RAS, TELEMAC-2D, or MIKE FLOOD, to simulate inundation extent and depth based on specific extreme precipitation scenarios (Beden and Ulke Keskin, 2021; Belhajjam et al., 2024; Tufano et al., 2023). However, contemporary research increasingly adopts Multi-Criteria Decision Analysis, specifically the Analytic Hierarchy Process (AHP) (Balado and Solla, 2024) and TOPSIS (Pathan et al., 2022), to systematically weight and fuse diverse geospatial layers. Furthermore, geomorphological descriptors like the Height Above Nearest Drainage (HAND) model are being integrated into web-based systems to provide computationally efficient, real-time inundation mapping across large scales (Li and Demir, 2022).

A significant technological advancement in the field is the integration of Machine Learning (ML) and Deep Learning (DL) to enhance predictive accuracy in flood susceptibility mapping (Singha et al., 2025). Algorithms such as Random Forest (RF), XGBoost, and Support Vector Machines (SVM) are frequently employed to model complex, non-linear relationships between hydrological triggers and topographical factors (Devi et al., 2025; Taromideh et al., 2022). Additionally, innovative applications of Generative Adversarial Networks (GANs) are used to synthesize realistic extreme precipitation patterns (Belhajjam et al., 2024). These models leverage high-resolution remote sensing data, including multitemporal Synthetic Aperture Radar (SAR) for cloud-penetrating monitoring and mobile LiDAR for building-level vulnerability assessments (Feng et al., 2022; Pramanick et al., 2022).

2.2 LiDAR and Point Cloud-based Flood Analysis

Point cloud technology, derived from LiDAR or photogrammetry, provides high-density, centimetre-level accuracy 3D geospatial data in flood management (Dimitrov et al., 2024; Jakovljevic et al., 2019). These dense point clouds are primarily utilized to generate high-resolution Digital Terrain Models (DTMs) and Digital Elevation Models (DEMs), which constitute the foundational geometry required for hydrological simulation models. Beyond basic topography, point clouds enable a fine-grained analysis of urban vulnerability by facilitating the extraction of specific structural features (building façades openings and elevations) (Guo et al., 2022). This allows researchers to automatically identify potential points of water ingress and quantify per-building risk levels by comparing detection heights with predicted flood water levels. Furthermore, point clouds are essential for monitoring the structural integrity of critical infrastructure, such as identifying levee deformations and depressions that could lead to structural failure (Wang et al., 2024). Their integration into Virtual Reality (VR) and GIS platforms also provides immersive environments for stakeholders to visualize various flooding scenarios, thereby enhancing collaborative decision-making and emergency response planning (Papadopoulou and Papakonstantinou, 2024).

Nevertheless, point clouds also function as an analytical output within change detection and deformation analysis processes; for instance, processed point clouds are employed to directly visualize and quantify levee depressions (Wang et al., 2024) or to identify mobile objects that represent potential hazards in flood-prone areas (Kögel and Carstensen, 2025). Consequently, ALS technology acts as both a robust data infrastructure (model) and a medium for visually representing risk assessments within immersive VR environments. This study will use point clouds not only as a data source, but also as the final output, enriching the point clouds with risk-related information.

3. Methodology

The proposed method relies on the extraction and combination of geometric features and relative elevation metrics derived from Aerial Laser Scanning (ALS) point clouds to estimate two key processes associated with extreme rainfall events (Figure 1). Runoff and water accumulation directly influence the generation and spatial distribution of urban flooding. Intense precipitation can exceed the infiltration and drainage capacities of the terrain and stormwater infrastructure, leading to rapid surface runoff and the concentration of water in topographic depressions and low-lying areas. The analysis of runoff pathways and water accumulation patterns therefore provides valuable information for identifying flood-prone zones, evaluating drainage performance, and estimating potential impacts on urban infrastructure and populations.

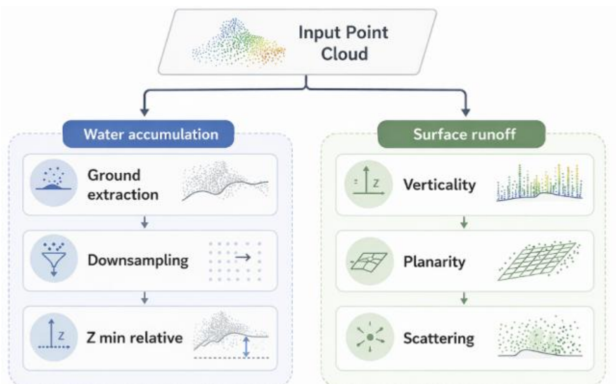

Figure 1. Workflow of the proposed method.

3.1 Water accumulation

For this estimate water accumulation, the method is based on previous studies that apply DEM-based flood modelling using moving windows (Guo et al., 2025; Kametaka et al., 2025). Similarly to these approaches, the elevation of each point P_i is compared with the minimum elevation within a search radius r_1. Specifically, the relative height is computed as the difference between the elevation of the point and the minimum elevation found within this neighbourhood (Eq. 1). This assumption relies on the principle that water preferentially flows towards and accumulates in topographically lower areas. Consequently, analysing relative elevation within a local neighbourhood provides a simple yet effective proxy for identifying potential water accumulation zones and runoff pathways.

$$ACU(x,y,z) = z - min\left\{z_i \middle| \sqrt{(x_i-x)^2+(y_i-y)^2} \leq r1\right\} \quad (1)$$

The search radius r_1 is defined as a neighbourhood of 100 m to capture terrain depressions and drainage structures whose spatial extent exceeds the scale typically considered in local geometric analyses. While previous studies frequently employ neighbourhoods of up to 15 m (Kametaka et al., 2025), such ranges mainly characterize fine-scale surface geometry and may fail to represent broader topographic contexts relevant to water accumulation processes. By extending the neighbourhood to 100 m, the proposed method incorporates a wider spatial context, enabling the detection of larger depressions and urban drainage patterns. However, due to the large number of points involved within such a neighbourhood, several optimization strategies were implemented to improve computational efficiency.

First, neighbourhood searches are performed in the XY plane to reduce computational complexity. In addition, taking advantage of the classification available in the point clouds used as case studies, it is assumed that the lowest elevations correspond to points labelled as "ground". Therefore, the neighbourhood search is restricted to these ground points. Furthermore, the density of the ground point cloud is reduced by generating a subsampled grid with a spacing of 10 m, which accelerates the search process.

3.2 Runoff

Surface runoff is strongly influenced by the geometric configuration of urban surfaces, as water flow is controlled by slope, surface continuity, and the presence of obstacles. For this reason, geometric features derived from point cloud analysis provide valuable information for identifying surfaces that facilitate or hinder water movement. Three geometric descriptors are considered: verticality, planarity, and scattering.

- Verticality provides a measure of local slope, which directly influences the speed and direction of surface water flow. To better capture the subtle inclinations that are most common in urban ground surfaces, the linear verticality values are transformed using a power function with an exponent of 0.1. This scaling enhances the contribution of small slopes that govern runoff across urban ground (roads, sidewalks, etc.).
- Planarity is used to identify continuous flat surfaces such as roads, pavements, and other ground elements that can facilitate the propagation of surface runoff. Flat, planar surfaces offer low resistance to water flow and therefore tend to channel runoff more effectively than irregular or discontinuous geometries. Changes in planarity often indicate the presence of obstacles (curbs, street furniture, etc.) that interrupt the continuity of the surface and can impede or redirect water flow.
- Scattering characterises irregular or highly rough geometries, such as vegetation or cluttered urban elements, where water flow may be dispersed or locally retained.

Together, these three factors provide a geometric representation of the urban environment that helps estimate potential runoff behaviour during extreme rainfall events. Verticality is computed based on the Z-component of the local surface normal N (Eq. 2). Planarity and scattering are derived from the eigenvalues of the covariance matrix and the eigenvalues (Eq. 3 to Eq. 7).

$$verticality = 1 - N_z \tag{2}$$

$$C = \frac{1}{k}\sum_{i=1}^{k}\begin{bmatrix} x_i - \bar{x} \\ y_i - \bar{y} \\ z_i - \bar{z} \end{bmatrix}\begin{bmatrix} x_i - \bar{x} & y_i - \bar{y} & z_i - \bar{z} \end{bmatrix} \tag{3}$$

$$det(C - \lambda I) = 0 \tag{4}$$

$$planarity = \frac{\lambda_2 - \lambda_1}{\lambda_3} \tag{5}$$

$$scattering = \frac{\lambda_1}{\lambda_3} \tag{6}$$

$$RUN(P) = \left(verticality(P)\right)^{0.1} \cdot planarity(P) \cdot |scattering(P) - 1| \tag{7}$$

4. Results and discussion

4.1 Case Studies

The proposed method was evaluated using ALS datasets from three cities with diverse urban typologies: Vigo (Spain), Rotterdam (The Netherlands), and Hong Kong (China). These study areas encompass a range of morphological characteristics, representing markedly different urban forms, densities, and spatial configurations. Vigo is characterized by a medium-density urban fabric adapted to a complex coastal topography, with significant elevation changes and a mixture of historic and contemporary developments. Rotterdam, in contrast, exhibits a predominantly flat terrain and a highly planned urban structure, featuring extensive modern architecture, large transportation infrastructures, and port-related facilities. Hong Kong presents an extreme case of vertical urbanization, where very high-rise and high-density developments coexist with steep mountainous terrain, creating a highly complex three-dimensional urban environment. Climatically, the three cities also differ substantially, with Vigo experiencing an oceanic climate, Rotterdam a temperate maritime climate, and Hong Kong a humid subtropical climate influenced by monsoonal patterns. These variations provide a diverse set of environmental and

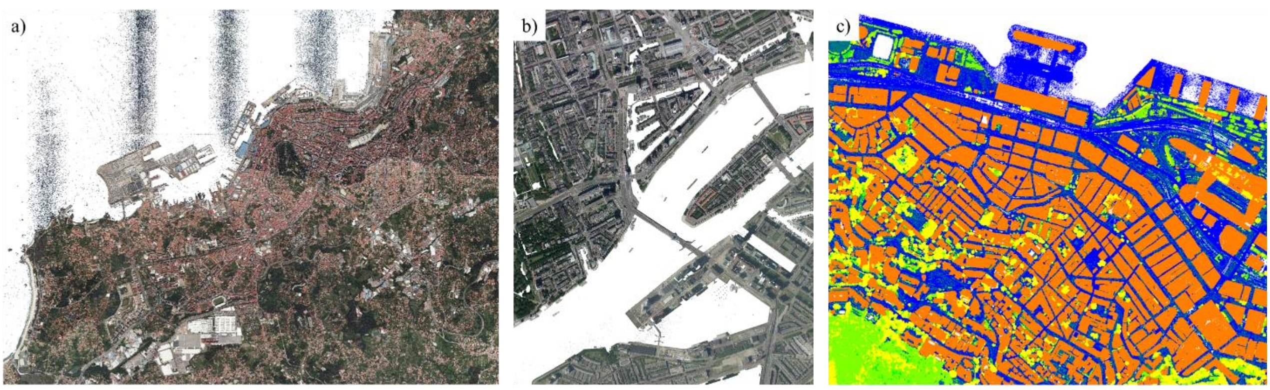

Figure 2. Input ALS point clouds: a) Vigo in real colour, b) Rotterdam in real colour, c) Hong Kong using colours according to the classification.

urban conditions for analysis while also benefiting from the availability of openly accessible point cloud datasets, which facilitate reproducibility and comparative assessment across distinct geographic and socio-environmental contexts. The input point clouds are presented in Figure 2. Each point cloud exhibits distinct point densities and structural complexity, reflecting differences in acquisition sources and urban form. Characteristics of each point cloud are presented in Table 1. Each dataset was downloaded from:

- Vigo: (Instituto Geográfico Nacional, 2026)
- Rotterdam: (GeoTiles, 2026)
- Hong Kong: (CEDD, 2026)

	Vigo	Rotterdam	Hong Kong
no. points	29M points	68M points	67M points
Coverage (m)	8000 ×6000	2000×2500	1500×1200
Point density (points/m²)	0.5 ~ 2	10 ~ 20	4 ~ 5
no. ground points (after downsampling)	261K points	39K points	9K points

Table 1. Characteristics of each point cloud.

All computations were performed on a computer equipped with an Intel® Core™ i9-13980HX CPU (2.20 GHz) and 32 GB of RAM, using MATLAB® for algorithm implementation and CloudCompare for point cloud processing/visualization. Processing times and search parameters for each dataset are presented in Table 2. The computation of geometric features was performed using a neighbourhood radius r_2 adapted to the point density of each cloud. Among the case studies, the Rotterdam dataset (AHN3 programme) exhibited the highest point density, requiring a smaller radius.

	Vigo	Rotterdam	Hong Kong
r_1	100 m	100 m	100 m
r_2	10 m	2 m	5 m
Processing time	26 min	32 min	2 min

Table 2. Processing thresholds and times.

4.2 Results

To improve the visualization of water accumulation in the point clouds, the maximum flood depth displayed (represented using a colour gradient) is limited to 10 m, corresponding to extreme flooding events in large rivers (Sangwai and Nagne, 2025; Shakti P. C. et al., 2022). However, floods associated with extreme rainfall events typically reach maximum depths of around 2 m (Iliadis et al., 2023; Li et al., 2025; Xu et al., 2025; Zhang et al., 2025). The enriched point clouds containing water accumulation and runoff information are shown in Figures 3 to 6.

With respect to water accumulation, relative depressions within the 100 m-local neighbourhood were successfully identified, allowing the accurate detection of low-lying areas. These include zones located near the harbours as well as semi-tunnel structures, where water accumulation is more likely to occur. Furthermore, the three-dimensional representation of the enriched point clouds enables a clear identification of elevated and potentially safe areas, even within locations characterized by higher flood risk.

Potential runoff areas were successfully identified across all case studies. These areas are characterized by inclined surfaces, no presence of objects that may influence or redirect water flow, and the absence of vegetation. The most prominent features correspond to sloped roofs, which facilitate effective drainage towards the stormwater network. In addition, extensive areas such as stairways, roads, and pedestrian ramps were clearly

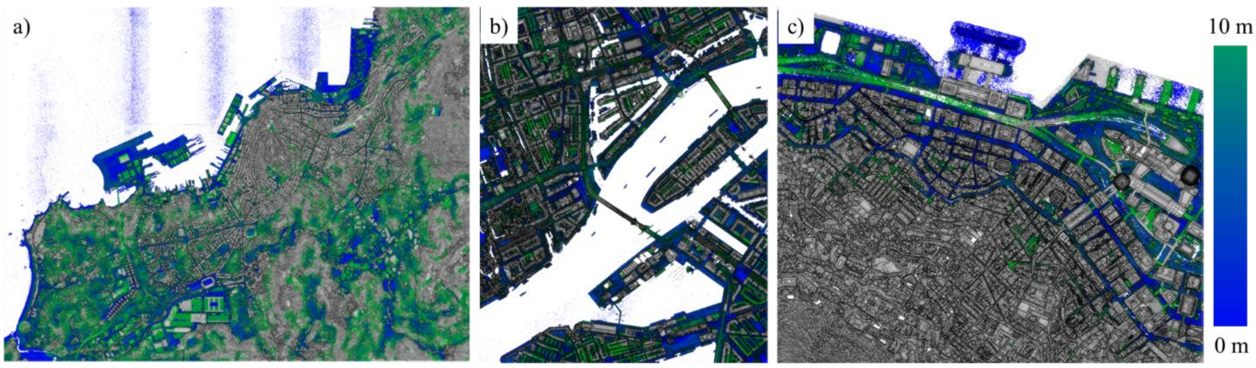

Figure 3. Top view of coloured ALS point cloud according water accumulation levels: a) Vigo, b) Rotterdam, c) Hong Kong.

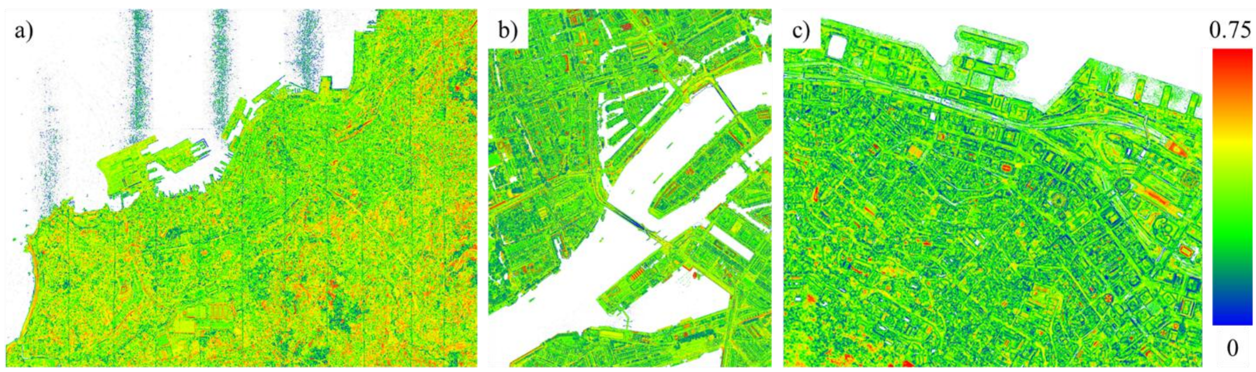

Figure 4. Top view of coloured ALS point cloud according runoff risk a) Vigo, b) Rotterdam, c) Hong Kong.

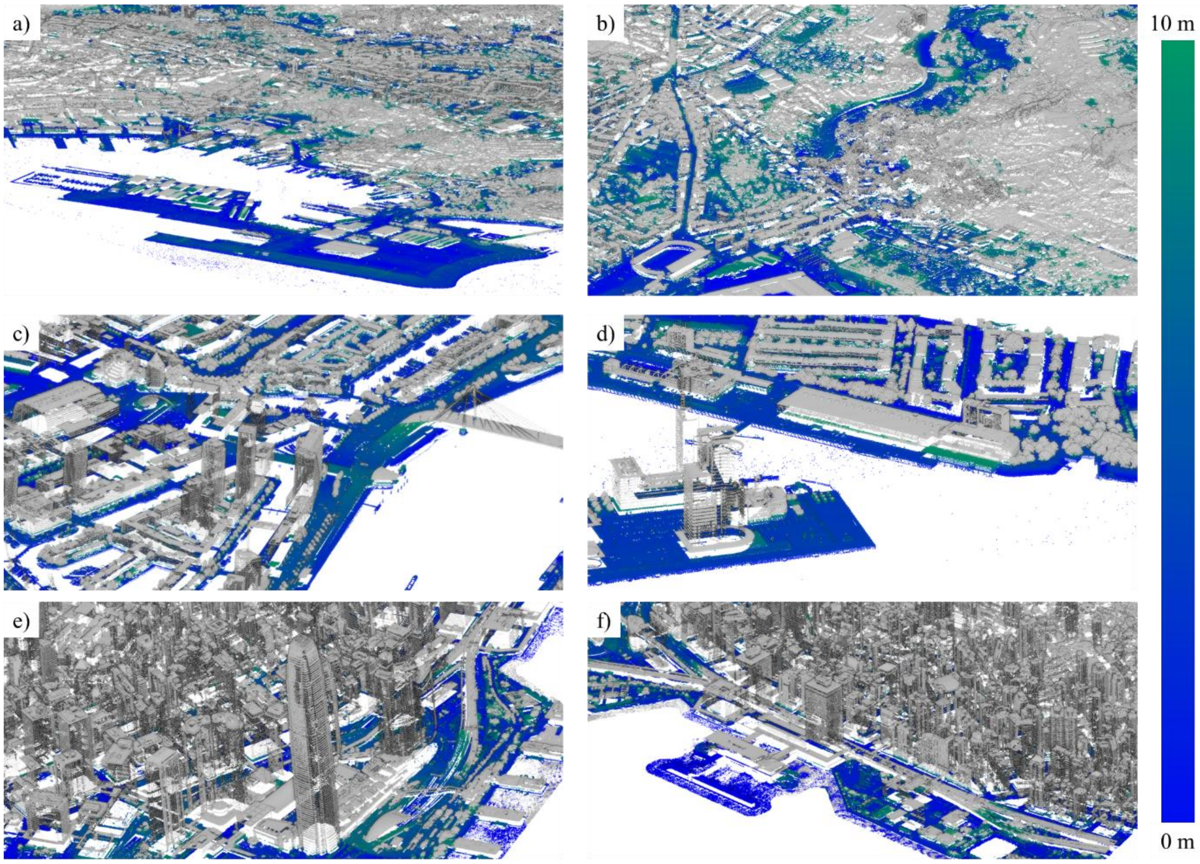

Figure 5. Coloured ALS point cloud according water accumulation levels: a-b) Vigo, c-d) Rotterdam, e-f) Hong Kong.

detected, as their geometric characteristics make them relevant pathways for surface runoff.

4.3 Discussion

Using the point cloud data, flood-related risks were accurately identified. In comparison with the study by (Balado and Solla, 2024), where risk maps were generated using AHP-GIS method, the geometrically and topographically derived risk zones show strong correspondence. Specifically, these include stadium areas, which are low-lying relative to their surroundings and intersected by a river; canyon-like avenues, characterized by excavated terrain and significant slopes on the surrounding embankments; and urban areas near the harbours, located beneath inclined zones that concentrate most of the population. Historically, these areas have also been affected by flooding and runoff events, confirming the reliability of the point cloud-based identification of hazard-prone zones. In comparison with previous studies in the other cities, the spatial distribution of flood risk identified through the proposed methodology also exhibits significant alignment with risk maps in Rotterdam (Dartée et al., 2023) and Hong Kong (Singh and Cai, 2023). This correspondence is particularly evident in the identification of critical low-lying harbor areas.

Transitioning from traditional 2D mapping to a direct 3D point cloud approach offers a significant advantage in capturing the inherent verticality of modern urban environments. While 2D models often rely on coarse resolutions that overlook critical vertical obstacles, such as building façades, archways, or boundary walls, the proposed 3D representation enables a more realistic assessment of how water interacts with complex structures like urban canyons and multi-level pathways. Furthermore, the scalability of the proposed methodology is demonstrated by its adaptability to the varying urban and point geometric characteristics and point densities inherent to different ALS sensors, as evidenced in the successful application across the contrasting morphologies of Vigo, Rotterdam, and Hong Kong.

Despite the successful identification of flood and runoff-prone areas, several limitations should be acknowledged. Large roofs are occasionally misclassified as low-lying areas because their central portions exceed the neighbourhood search window, leading to local errors in water accumulation detection. Similarly, areas with sparse ALS coverage, such as the ground surfaces in urban canyons, may result in incomplete or less reliable measurements. The current approach does not account for the dynamics of floating or movable elements, including docks, boats, or temporary barriers, which can influence flow paths.

Additional limitations include the inability to capture subsurface drainage networks, potential errors in vegetation filtering that may obscure the true terrain, and the static nature of the analysis, which does not consider temporal variations in rainfall intensity or water levels. These factors should be considered when interpreting the results and planning for practical applications in urban flood risk management.

5. Conclusion

Urban floods pose significant risks to cities, highlighting the need for accurate spatial assessment and visualization methods to support risk management and mitigation. This research demonstrates that Aerial Laser Scanning (ALS) point clouds can serve as a direct analytical medium for 3D flood risk mapping,

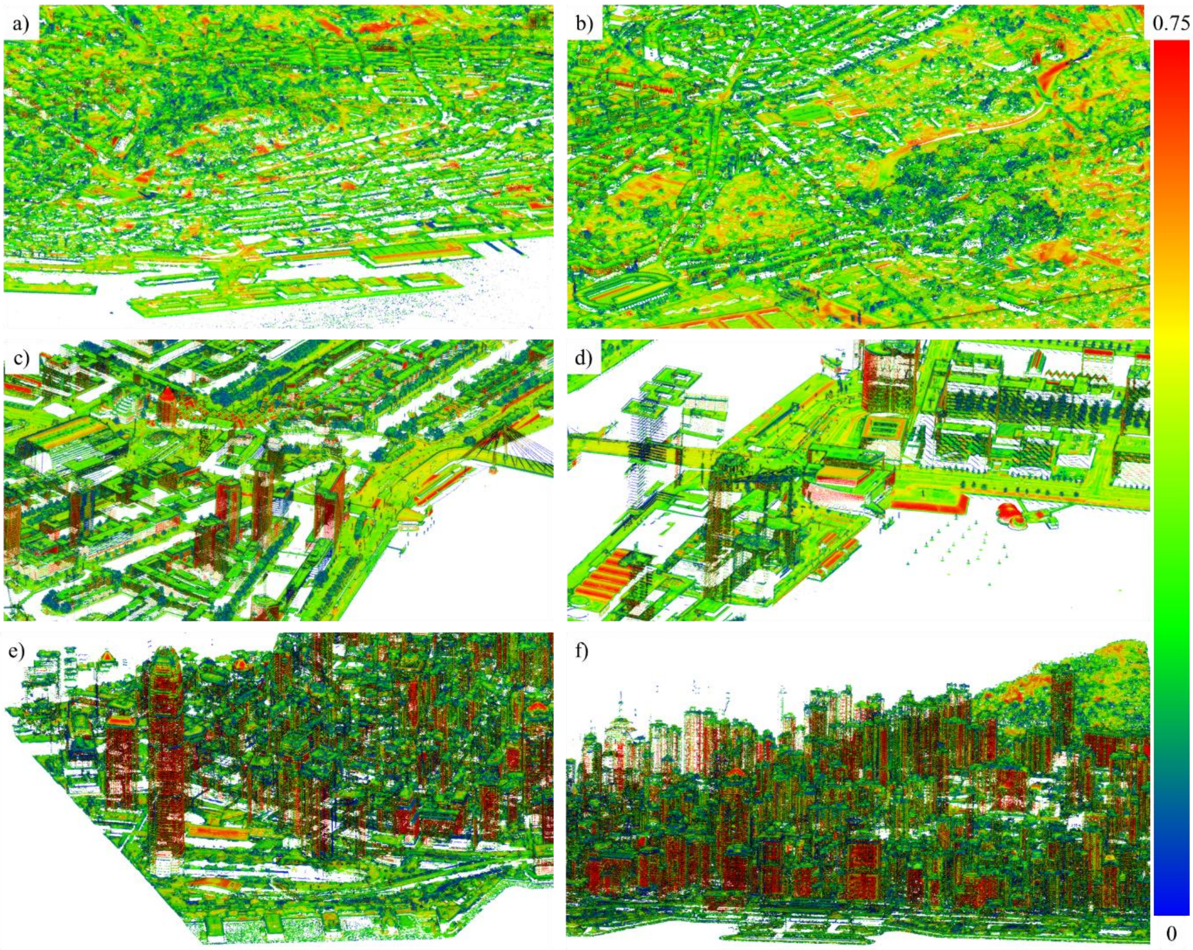

Figure 6. Coloured ALS point cloud according runoff risk: a-b) Vigo, c-d) Rotterdam, e-f) Hong Kong.

eliminating the need for intermediate surface reconstruction. By integrating elevation-based indicators for water accumulation and geometric descriptors (verticality, planarity, and scattering) for runoff potential, the proposed methodology successfully identified critical urban features across three diverse morphologies: Vigo, Rotterdam, and Hong Kong. The evidence indicates that the model accurately maps flood-prone zones, such as low-lying harbour areas and urban canyons, as well as runoff pathways including sloped roofs, stairways, and ramps, which are often simplified in traditional 2D models.

The validation of these results against historical flood events and established multi-criteria assessments (AHP-GIS) confirms the reliability of using point-level enrichment to detect hazard-prone zones. While limitations remain regarding subsurface drainage and large-scale roof misclassifications, the study proves that preserving the full geometric richness of LiDAR data enhances the visual intuition and spatial precision of urban flood management tools

Future work will focus on integrating additional data sources, such as drainage networks and real-time hydrological measurements, to improve the accuracy and predictive capability of the models. A systematic sensitivity analysis of the key parameters will be essential to evaluate the robustness and generalizability of the proposed framework across diverse urban contexts. Investigating the impact of varying the neighbourhood search radii (the 100-m threshold for water accumulation r_1 and the density-adapted radii r_2) will clarify how different spatial scales influence the detection of topographic depressions and micro-runoff pathways. Moreover, given the large volume points in ALS data, further optimization of the computational workflow is needed to enhance processing efficiency and scalability, enabling broader application to complex urban environments. The code implementation is publicly available on GitHub (Balado Frías, 2026).

Acknowledgments

J. Balado acknowledges the grant RYC2022-038100-I funded by MCIN/AEI/10.13039/501100011033 and FSE+; and from Xunta de Galicia - GAIN [EDC431C 2024/30].

References

Balado Frías, J., 2026. ALS_Flood3D . URL https://github.com/jbalado/ALS_Flood3D (accessed 7.12.26).

Balado, J., Solla, M., 2024. Multi-Criteria GIS for Sponge City Planning with Open Data Sources in Vigo (Spain). ISPRS Annals of the Photogrammetry, Remote Sensing and Spatial Information Sciences X-4/W5-2024, 41–48. https://doi.org/10.5194/isprs-annals-X-4-W5-2024-41-2024

Baptista, M.D., Livesley, S.J., G. Parmehr, E., Neave, M., Amati, M., 2018. Terrestrial Laser Scanning to Predict Canopy Area Metrics, Water Storage Capacity, and Throughfall Redistribution in Small Trees. Remote Sensing 10, 1958. https://doi.org/10.3390/rs10121958

Beden, N., Ulke Keskin, A., 2021. Flood map production and evaluation of flood risks in situations of insufficient flow data. Natural Hazards 105, 2381–2408. https://doi.org/10.1007/s11069-020-04404-y

Belhajjam, R., Chaqdid, A., Yebari, N., Seaid, M., El Moçayd, N., 2024. Climate-informed flood risk mapping using a GAN-based approach (ExGAN). Journal of Hydrology 638, 131487. https://doi.org/10.1016/j.jhydrol.2024.131487

Bui, Q.D., Luu, C., Mai, S.H., Ha, H.T., Ta, H.T., Pham, B.T., 2023. Flood risk mapping and analysis using an integrated framework of machine learning models and analytic hierarchy process. Risk Analysis 43, 1478–1495. https://doi.org/10.1111/risa.14018

CEDD, 2026. Spatial Data Portal [WWW Document]. URL https://sdportal.cedd.gov.hk/#/ (accessed 3.12.26).

Costabile, P., Costanzo, C., De Lorenzo, G., De Santis, R., Penna, N., Macchione, F., 2021. Terrestrial and airborne laser scanning and 2-D modelling for 3-D flood hazard maps in urban areas: new opportunities and perspectives. Environmental Modelling & Software 135, 104889. https://doi.org/10.1016/j.envsoft.2020.104889

Dartée, K.W.J., Biffin, T., Peña, K., 2023. The Opportunities and Challenges for Urban NBS: Lessons from Implementing the Urban Waterbuffer in Rotterdam, in: López-Gunn, E., van der Keur, P., Van Cauwenbergh, N., Le Coent, P., Giordano, R. (Eds.), Greening Water Risks: Natural Assurance Schemes. Springer International Publishing, Cham, pp. 325–345. https://doi.org/10.1007/978-3-031-25308-9_16

Devi, K., Reddy, C.C., Rahul, K., Khuntia, J.R., Das, B.S., 2025. A holistic methodology for evaluating flood vulnerability, generating flood risk map and conducting detailed flood inundation assessment. Scientific Reports 15, 28253. https://doi.org/10.1038/s41598-025-13025-z

Dimitrov, S., Borisova, B., Ihtimanski, I., Radeva, K., Iliev, M., Semerdzhieva, L., Petrov, S., 2024. Rapid Mapping: Unmanned Aerial Vehicles and Mobile-Based Remote Sensing for Flash Flood Consequence Monitoring (A Case Study of Tsarevo Municipality, South Bulgarian Black Sea Coast). Urban Science 8, 255. https://doi.org/10.3390/urbansci8040255

Feng, Y., Xiao, Q., Brenner, C., Peche, A., Yang, J., Feuerhake, U., Sester, M., 2022. Determination of building flood risk maps from LiDAR mobile mapping data. Computers, Environment and Urban Systems 93, 101759. https://doi.org/10.1016/j.compenvurbsys.2022.101759

GeoTiles, 2026. GeoTiles [WWW Document]. URL https://geotiles.nl/ (accessed 3.12.26).

Guo, M., Gong, J., Whytlaw, J.L., 2022. Large-scale cloud-based building elevation data extraction and flood insurance estimation to support floodplain management. International Journal of Disaster Risk Reduction 69, 102741. https://doi.org/10.1016/j.ijdrr.2021.102741

Guo, X., Wang, Q.J., Western, A., Ryu, D., Sharples, W., Hou, J., 2025. Flood monitoring: A hydrologically guided method for infilling incomplete flood inundation maps derived from satellite images. Journal of Hydrology 660, 133365. https://doi.org/10.1016/j.jhydrol.2025.133365

Huang, H., Tian, Y., Wei, M., Jia, X., Wang, P., Ackerman, A.C., Chatterjee, S.G., Liu, Y., Tian, G., 2023. A Theoretical Nonlinear Regression Model of Rainfall Surface Flow Accumulation and Basin Features in Park-Scale Urban Green Spaces Based on LiDAR Data. Water 15, 2442. https://doi.org/10.3390/w15132442

Iliadis, C., Galiatsatou, P., Glenis, V., Prinos, P., Kilsby, C., 2023. Urban Flood Modelling under Extreme Rainfall Conditions for Building-Level Flood Exposure Analysis. Hydrology 10, 172. https://doi.org/10.3390/hydrology10080172

Instituto Geográfico Nacional, 2026. Centro de Descargas del CNIG (IGN) [WWW Document]. Centro de Descargas del CNIG. URL http://centrodedescargas.cnig.es (accessed 3.12.26).

Jakovljevic, G., Govedarica, M., Alvarez-Taboada, F., Pajic, V., 2019. Accuracy Assessment of Deep Learning Based Classification of LiDAR and UAV Points Clouds for DTM Creation and Flood Risk Mapping. Geosciences 9, 323. https://doi.org/10.3390/geosciences9070323

Kametaka, R., Adriano, B., Mas, E., Koshimura, S., 2025. Accurate flood extent mapping in suburban areas using a single SAR image: FFT-based artifact removal approach. International Journal of Applied Earth Observation and Geoinformation 144, 104941. https://doi.org/10.1016/j.jag.2025.104941

Kögel, M., Carstensen, D., 2025. Near real-time change detection tool for photogrammetric flood preparedness. Environmental Monitoring and Assessment 197, 129. https://doi.org/10.1007/s10661-024-13597-9

Li, G., Wu, X., Han, J.-C., Li, B., Huang, Y., Wang, Y., 2023. Flood risk assessment by using an interpretative structural modeling based Bayesian network approach (ISM-BN): An urban-level analysis of Shenzhen, China. Journal of Environmental Management 329, 117040. https://doi.org/10.1016/j.jenvman.2022.117040

Li, Y., Wang, L., Li, F., Peng, S.G., Ding, C., 2025. Quantitative estimation of urban flood damage from storm surges for a coastal city. Natural Hazards 121, 16915–16934. https://doi.org/10.1007/s11069-025-07456-0

Li, Z., Demir, I., 2022. A comprehensive web-based system for flood inundation map generation and comparative analysis based on height above nearest drainage. Science of The Total Environment 828, 154420. https://doi.org/10.1016/j.scitotenv.2022.154420

Öztürk, Ş., Yılmaz, K., Dinçer, A.E., Kalpakcı, V., 2024. Effect of urbanization on surface runoff and performance of green roofs and permeable pavement for mitigating urban floods. Natural Hazards 120, 12375–12399. https://doi.org/10.1007/s11069-024-06688-w

Papadopoulou, E.E., Papakonstantinou, A., 2024. Combining Drone LiDAR and Virtual Reality Geovisualizations towards a

Cartographic Approach to Visualize Flooding Scenarios. Drones 8. https://doi.org/10.3390/drones8080398

Pathan, A.I., Girish Agnihotri, P., Said, S., Patel, D., 2022. AHP and TOPSIS based flood risk assessment- a case study of the Navsari City, Gujarat, India. Environmental Monitoring and Assessment 194, 509. https://doi.org/10.1007/s10661-022-10111-x

Pramanick, N., Acharyya, R., Mukherjee, Sandip, Mukherjee, Sudipta, Pal, I., Mitra, D., Mukhopadhyay, A., 2022. SAR based flood risk analysis: A case study Kerala flood 2018. Advances in Space Research 69, 1915–1929. https://doi.org/10.1016/j.asr.2021.07.003

Rehman, S., Sahana, M., Hong, H., Sajjad, H., Ahmed, B.B., 2019. A systematic review on approaches and methods used for flood vulnerability assessment: framework for future research. Natural Hazards 96, 975–998. https://doi.org/10.1007/s11069-018-03567-z

Sangwai, A., Nagne, A., 2025. Mathematical and Hydraulic Analysis of Flood Events Using HEC- RAS in the River Basin: A Case Study. Panamerican Mathematical Journal. https://doi.org/10.52783/pmj.v35.i4s.5951

Shakti P. C., Miyamoto, M., Kakinuma, D., Misumi, R., Sriariyawat, A., Visessri, S., 2022. Probable Flood Inundation Depth and Extent in the Chao Phraya River Basin for Different Return Periods. Journal of Disaster Research 17, 901–912. https://doi.org/10.20965/jdr.2022.p0901

Singh, M., Cai, X., 2023. Coastal Flooding Hazard, Exposure, and Readiness of Buildings in Hong Kong in 2080–2100, and the Implications for Real Estate Management. ISPRS International Journal of Geo-Information 12. https://doi.org/10.3390/ijgi12030086

Singha, C., Sahoo, S., Mahtaj, A.B., Moghimi, A., Welzel, M., Govind, A., 2025. Advancing flood risk assessment: Multitemporal SAR-based flood inventory generation using transfer learning and hybrid fuzzy-AHP-machine learning for flood susceptibility mapping in the Mahananda River Basin. Journal of Environmental Management 380, 124972. https://doi.org/10.1016/j.jenvman.2025.124972

Spiridonov, V., Ćurić, M., Novkovski, N., 2025. Exploring Natural Hazards: From Earthquakes, Floods, and Beyond, in: Spiridonov, V., Ćurić, M., Novkovski, N. (Eds.), Atmospheric Perspectives: Unveiling Earth's Environmental Challenges. Springer Nature Switzerland, Cham, pp. 271–306. https://doi.org/10.1007/978-3-031-86757-6_11

Taromideh, F., Fazloula, R., Choubin, B., Emadi, A., Berndtsson, R., 2022. Urban Flood-Risk Assessment: Integration of Decision-Making and Machine Learning. Sustainability 14, 4483. https://doi.org/10.3390/su14084483

Tokarčík, O., Hofierka, J., 2024. Designing flash flood control measures for urban areas using the Monte Carlo water flow simulation. Geomatics, Natural Hazards and Risk 15, 2361806. https://doi.org/10.1080/19475705.2024.2361806

Trepekli, K., Balstrøm, T., Friborg, T., Fog, B., Allotey, A.N., Kofie, R.Y., Møller-Jensen, L., 2022. UAV-borne, LiDAR-based elevation modelling: a method for improving local-scale urban flood risk assessment. Natural Hazards 113, 423–451. https://doi.org/10.1007/s11069-022-05308-9

Tufano, R., Guerriero, L., Annibali Corona, M., Cianflone, G., Di Martire, D., Ietto, F., Novellino, A., Rispoli, C., Zito, C., Calcaterra, D., 2023. Multiscenario flood hazard assessment using probabilistic runoff hydrograph estimation and 2D hydrodynamic modelling. Natural Hazards 116, 1029–1051. https://doi.org/10.1007/s11069-022-05710-3

Waghwala, R.K., Agnihotri, P.G., 2019. Flood risk assessment and resilience strategies for flood risk management: A case study of Surat City. International Journal of Disaster Risk Reduction 40, 101155. https://doi.org/10.1016/j.ijdrr.2019.101155

Wang, X., Wang, Yidan, Liao, X., Huang, Y., Wang, Yuli, Ling, Y., Chan, T.O., 2024. Monitoring of Levee Deformation for Urban Flood Risk Management Using Airborne 3D Point Clouds. Water 16, 559. https://doi.org/10.3390/w16040559

Xu, Z., Wang, X., He, B., 2025. Hydrological and hydraulic modelling of flash flood induced by extreme rainfall in Liulin town, Hubei province, China, 2021. Engineering Applications of Computational Fluid Mechanics 19, 2562107. https://doi.org/10.1080/19942060.2025.2562107

Zhang, Y., Wang, L., Zhang, Q., Li, Y., Wang, P., Hu, T., 2025. A Comprehensive Analysis of Urban Flooding Under Different Rainfall Patterns: A Full-Process Perspective in Haining, China. Atmosphere 16, 305. https://doi.org/10.3390/atmos16030305